Journal of Magnetism and Magnetic Materials 363 (2014) 133–139

Contents lists available at ScienceDirect

Journal of Magnetism and Magnetic Materials

journal homepage: www.elsevier.com/locate/jmmm

Electronic structure, Fermi surface topology and spectroscopic optical properties of $LaBaCo_2O_{5.5}$ compound

A.H. Reshak [a,b], Y. Al-Douri [c], R. Khenata [d], Wilayat Khan [a], Saleem Ayaz Khan [a], Sikander Azam [a,*]

[a] New Technologies – Research Center, University of West Bohemia, Univerzitni 8, Pilsen 306 14, Czech Republic
[b] Center of Excellence Geopolymer and Green Technology, School of Material Engineering, University Malaysia Perlis, 01007 Kangar, Perlis, Malaysia
[c] Institute of Nano Electronic Engineering, University Malaysia Perlis, 01000 Kangar, Perlis, Malaysia
[d] Laboratoire de Physique Quantique et de Modélisation Mathématique (LPQ3M), Département de Technologie, Université de Mascara, Mascara 29000, Algeria

ARTICLE INFO

Article history:
Received 8 February 2014
Received in revised form
25 February 2014
Available online 31 March 2014

Keywords:
Metallic
DFT
Fermi surface
Optical property

ABSTRACT

We have investigated the electronic band structure, Fermi surface topology, chemical bonding and optical properties of $LaBaCo_2O_{5.5}$ compound. The first-principle calculations based on density functional theory (DFT) by means of the full-potential linearized augmented plane-wave method were employed. The atomic positions of $LaBaCo_2O_{5.5}$ compound were optimized by minimizing the forces acting on atoms. We employed the local density approximation (LDA), generalized gradient approximation (GGA) and Engel–Vosko GGA (EVGGA) to treat the exchange correlation potential by solving Kohn–Sham equations. Electronic structure and bonding properties are studied throughout the calculation of densities of states, Fermi surfaces and charge densities. Furthermore, the optical properties are investigated via the calculation of the dielectric tensor component in order to characterize the linear optical properties. Optical spectra are analyzed by means of the electronic structure, which provides theoretical understanding of the conduction mechanism of the investigated compound.

1. Introduction

During the last decade, oxygen scarce ordered double perovskite cobaltates with general formula $LnBaCo_2O_{5.5}$ (Ln=lanthanides or Y elements) have drawn key interest due to their own fascinating physical features [1–18]. These 112 cobalt perovskites display numerous magnetic transitions and paramagnetic (PM)/ferromagnetic (FM)/antiferromagnetic (AFM) properties in a spacious temperature range. In addition a semimetal/insulator transition is previewed in room temperature. A significant issue concerns possible existence of different spin configuration in cobalt which would describe both the magnetic and the semimetal–insulator transitions that are observed in these materials.

In addition to analysis of many authors [1–18] who recommend this important role of spin state transitions in such properties, there are other several reports which do not agree with the occurrence of spin state transition in these systems across T_{IM} [19–23].

Numerous neutron diffraction analyses have been conducted to set up the spin state of cobalt and magnetic structure in $LnBaCo_2O_{5.5}$ compounds with Ln=Pr, Nd, Tb, Ho, and Y [6,18,24–30]. The models premeditated for the magnetic structure of these compounds are all different, and there is conflict between two different studies on the same compound [6,18]. There are three potential reasons for these contradictions.

(i) Small deviations from ideal "$O_{5.5}$" stoichiometry, (ii) variation in the degree of ordering in oxygen vacancies due to different method of synthesis, and (iii) the influence of the size of Ln^{3+} cation. Rautama et al. [31] tried to synthesize the lanthanum-based $LaBaCo_2O_{5.5}$ phase, which was not known till now, and has the advantage of containing the nonmagnetic La^{3+} cation. Co ions in the heavy metal oxides show high sensitivity to the environment [32].

The rest of the paper has been divided into three parts. In Section 2, we briefly describe the computational method used in this study. Most relevant results obtained for the electronic and optical properties of $LaBaCo_2O_{5.5}$ are presented and discussed in Section 3. Finally, we summarize the main conclusions in Section 4.

2. Computational details

$LaBaCo_2O_{5.5}$ compound crystallizes in orthorhombic structure with the space group *pmmm* (No. 47). The unit cell and molecular

* Corresponding author.
E-mail address: sikander.physicst@gmail.com (S. Azam).

http://dx.doi.org/10.1016/j.jmmm.2014.03.069
0304-8853/

cell structure of $LaBaCo_2O_{5.5}$ is illustrated in Fig. 1. Our calculations were carried out by means of the full-potential linearized augmented plane-wave method (FPLAPW) as implemented in the WIEN2k [33]. Local density approximation (LDA) [34], generalized gradient approximation (GGA) [35] and Engel–Vosko GGA (EVGGA) [36] exchange–correlation potential were used. The plane-wave cutoff, defined by the product of the smallest atomic sphere radius times the magnitude of the largest reciprocal-lattice vector (RMT_{min},K_{max}), was set to 7.0. Atomic positions of $LaBaCo_2O_{5.5}$ compound were optimized by minimizing the forces acting on the atoms (see Table 1). Self-consistent calculations were considered to be converged when the difference in the total energy of the crystal did not exceed 0.01 mRy and the atomic forces did not exceed 1 mRy/a.u. Hybridization effects were analyzed using densities of states (DOSs), which were obtained by the modified tetrahedron method, and some peculiarities of inter-atomic bonding picture were visualized by means of charge density maps Table 1.

For the calculation of the optical properties, which usually requires a dense mesh of uniformly distributed **k**-points, the Brillouin zone integration was performed using the tetrahedron method with 500 **k**-points in the irreducible part of the Brillouin zone. The dielectric function ($\varepsilon(\omega)$) is known to describe the optical response of the medium at all photon energies.

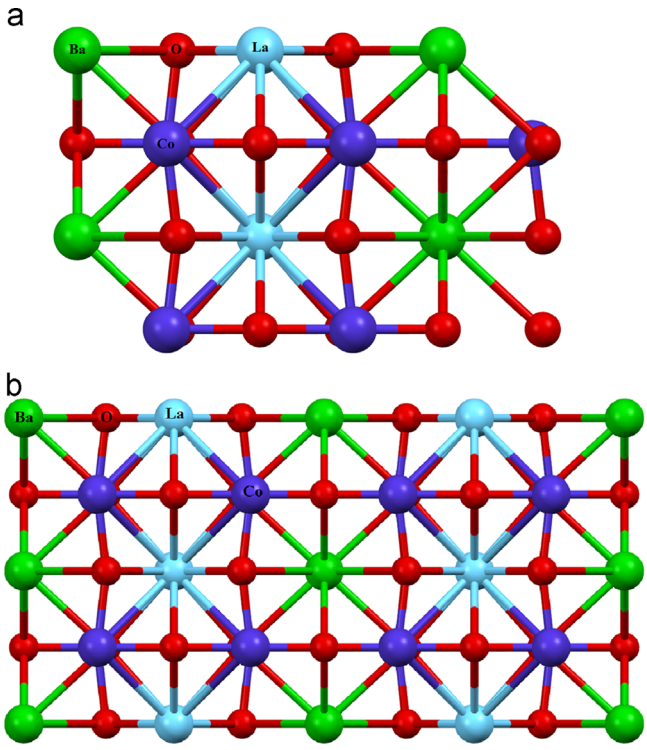

Fig. 1. Unit cell and molecular cell structure.

Table 1
Atomic positions of $LaBaCo_2O_{5.5}$ compound.

Atoms	X Exp.	X Opt.	Y Exp.	Y Opt.	Z Exp.	Z Opt.
La	0.5000	0.5000	0.6722	0.2491	0.0000	0.0000
Ba	0.5000	0.5000	0.2465	0.2508	0.5000	0.5000
Co1	0.0000	0.0000	0.0000	0.0000	0.244(1)	0.2553
Co2	0.0000	0.0000	0.5000	0.5000	0.259(1)	0.2548
O1	0.0000	0.0000	0.2358(6)	0.2498	0.2188(5)	0.2259
O2	0.5000	0.5000	0.0000	0.0000	0.2040(9)	0.2266
O3	0.5000	0.5000	0.5000	0.5000	0.2433(9)	0.2250
O4	0.0000	0.0000	0.0000	0.0000	0.5000	0.5000
O5	0.0000	0.0000	0.5000	0.5000	0.5000	0.5000
O6	0.0000	0.0000	0.5000	0.5000	0.0000	0.0000
O7	0.0000	0.0000	0.0000	0.0000	0.0000	0.0000

In metals, there are two contributions to dielectric function arising from the interband and intraband transitions. Interband transitions can be further split into direct and indirect transitions. However, both intraband and indirect interband transitions involve phonon in order to account for the momentum transfer. The intraband and indirect interband transition on the average add a rather smooth background to the spectra [14]. They have, therefore, been neglected in this study. The calculated direct interband contribution to the imaginary part of the dielectric function, $\varepsilon(\omega)$, is calculated by summing transitions from occupied to unoccupied states (with fixed wave vector) over the Brillouin zone, weighted with the appropriate matrix elements giving the probability for the transition. Specifically, in this study, the imaginary part of the dielectric function $\varepsilon(\omega)$ is given by the following expression [37]:

$$\varepsilon_2(\omega) = \left(\frac{4\pi^2 e^2}{m^2\omega^2}\right)\sum_{i,j}\int \langle i|M|j\rangle^2 f_i(1-f_j)\delta(E_f - E_i - \omega)d^3k \quad (1)$$

where M is the dipole matrix, i and j are the initial and final states, respectively, f_i is the Fermi distribution function for the ith state, and E_i is the energy of electron in the ith state. The real part ($\varepsilon(\omega)$) of the dielectric function can be evaluated from the imaginary part by using the Kramers–Kronig relation [38]

$$\mathrm{Re}[\varepsilon(\omega)] = \varepsilon_1(\omega) = 1 + \frac{2}{\pi}P\int_0^\infty \frac{\omega'\mathrm{Im}\varepsilon(\omega')}{\omega'^2-\omega^2}d\omega' \quad (2)$$

where P implies the principal value of the integral. The knowledge of both the real and imaginary parts of the dielectric tensor allows the calculation of other important optical functions. To this end, we also present and discuss the theoretically calculated optical conductivity ($\sigma(\omega)$) and reflectivity ($R(\omega)$) spectra of $LaBaCo_2O_{5.5}$. The real part of the optical conductivity $\mathrm{Re}(\sigma(\omega))$ is generally given by the equation given below. It is seen that the real part of the optical conductivity is essentially the imaginary part of the dielectric function scaled with the transition energy.

$$\mathrm{Re}[\sigma(\omega)] = \frac{\omega}{4\pi}\mathrm{Im}\varepsilon(\omega) \quad (3)$$

The reflectivity spectrum is derived from the Fresnel's formula for normal incidence assuming an orientation of the crystal surface parallel to the optical axis using the relation

$$R(\omega) = \left[\frac{\sqrt{\varepsilon(\omega)}-1}{\sqrt{\varepsilon(\omega)}+1}\right]^2 \quad (4)$$

3. Results and discussion

3.1. Electronic structure

The electronic band structure, Fermi surfaces, as well as total and site-projected l-decomposed densities of states (DOS) for the herein studied $LaBaCo_2O_{5.5}$ compound have been calculated at the equilibrium geometries. The calculated energy band structure along the high symmetry directions in the Brillouin zone and total densities of states (TDOS) are shown in Figs. 2 and 3. The valence and conduction bands overlap considerably around Fermi level. This suggests that $LaBaCo_2O_{5.5}$ compound would exhibit metallic conductivity. TDOS has a large finite value at the Fermi level, $N(E_F)$, which is equal to 28.76, 24.15 and 22.76 states/eV unit cell for LDA, GGA and EVGGA, respectively. Once again, this finding confirms the metallicity of this material. The obtained data also allow us to estimate Summerfield constants for $LaBaCo_2O_{5.5}$ under

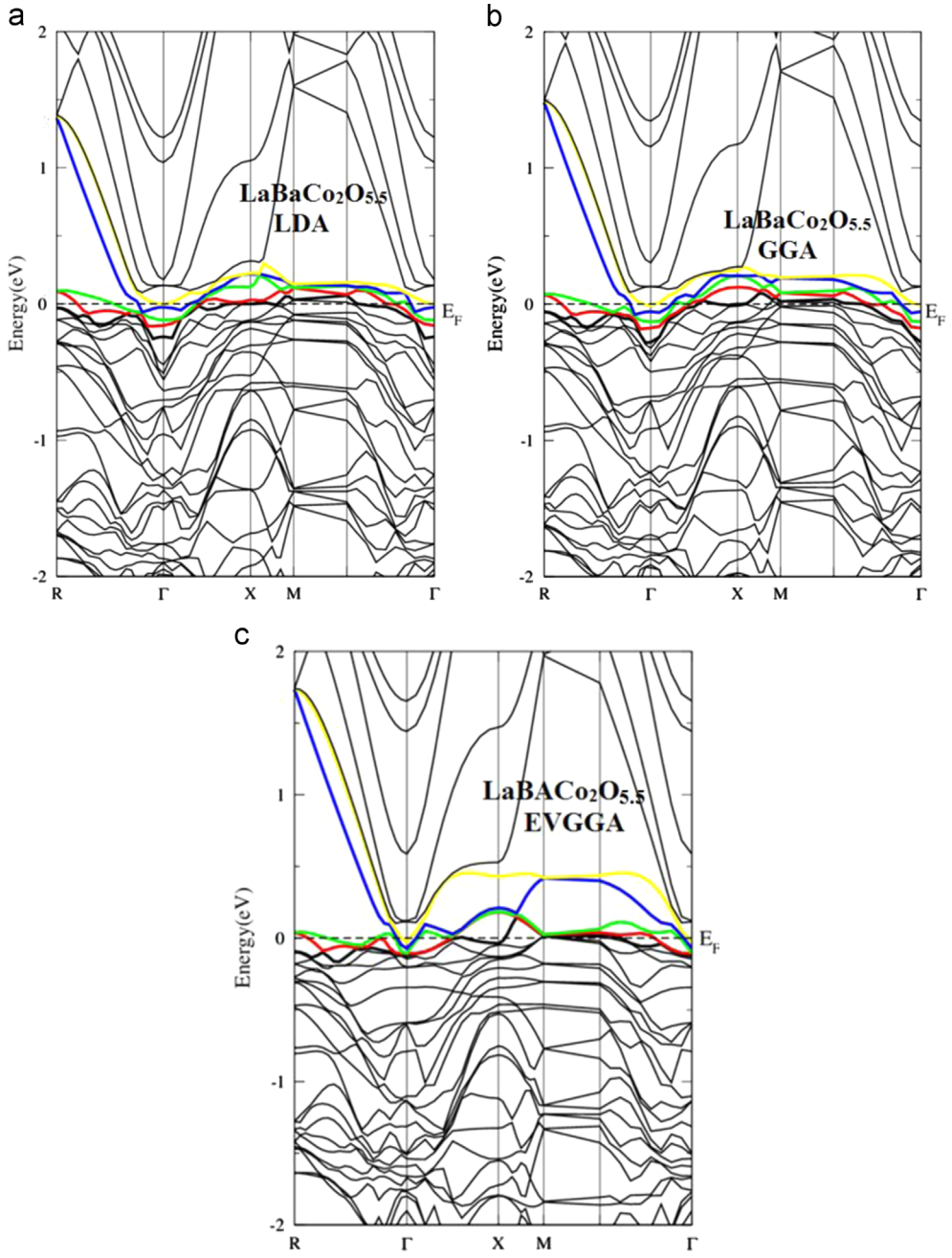

Fig. 2. Calculated band structure. (a) LDA, (b) GGA and (c) EVGGA and the color bands in the EVGGA shows that five bands cross the Fermi surface. (For interpretation of the references to color in this figure, the reader is referred to the web version of this article.)

the assumption of the free electron model as

$$\gamma = \frac{1}{3}\pi^2 N(E_F) K_\beta^2 \quad (5)$$

The calculated γ values are 4.98, 4.18 and 3.94 mJ/mol K^2 for LDA, GGA and EVGGA, respectively. In Figs. 2 and 3 total and partial density states (TDOS and PDOS) projected on each atomic species are represented. The total DOS shows a lot of structures that can be better understood by looking at the PDOS. From the PDOS we are able to identify the angular momentum character of the various structures. In the energy range from −6.0 eV to 3.0 eV the O p and Co d states represent the main contribution to the DOS, together with a contribution from La/Ba s and Co s/p states. For states ranging from −18.0 eV to −16.0 eV, all species are contributing to the DOS, whereas only La/Ba p states are responsible for the structure between −14.0 and −13 eV. At high energy (7.0–12.0 eV), the DOS is exclusively made from electronic states of the Ba/Co s and La/Ba d states with small contributions of Ba/La s states.

Fig. 2 shows the near-Fermi band structure of $LaBaCo_2O_{5.5}$ along the selected high-symmetry lines within the first Brillouin zone of the tetragonal crystal. It is seen that the Fermi level is crossed by Co 3d bands, which indicates that the electrical conductivity of this phase should be metallic. It is well established that electronic states crossing the Fermi level are primarily responsible for the Fermi surface (FS) structure and are always

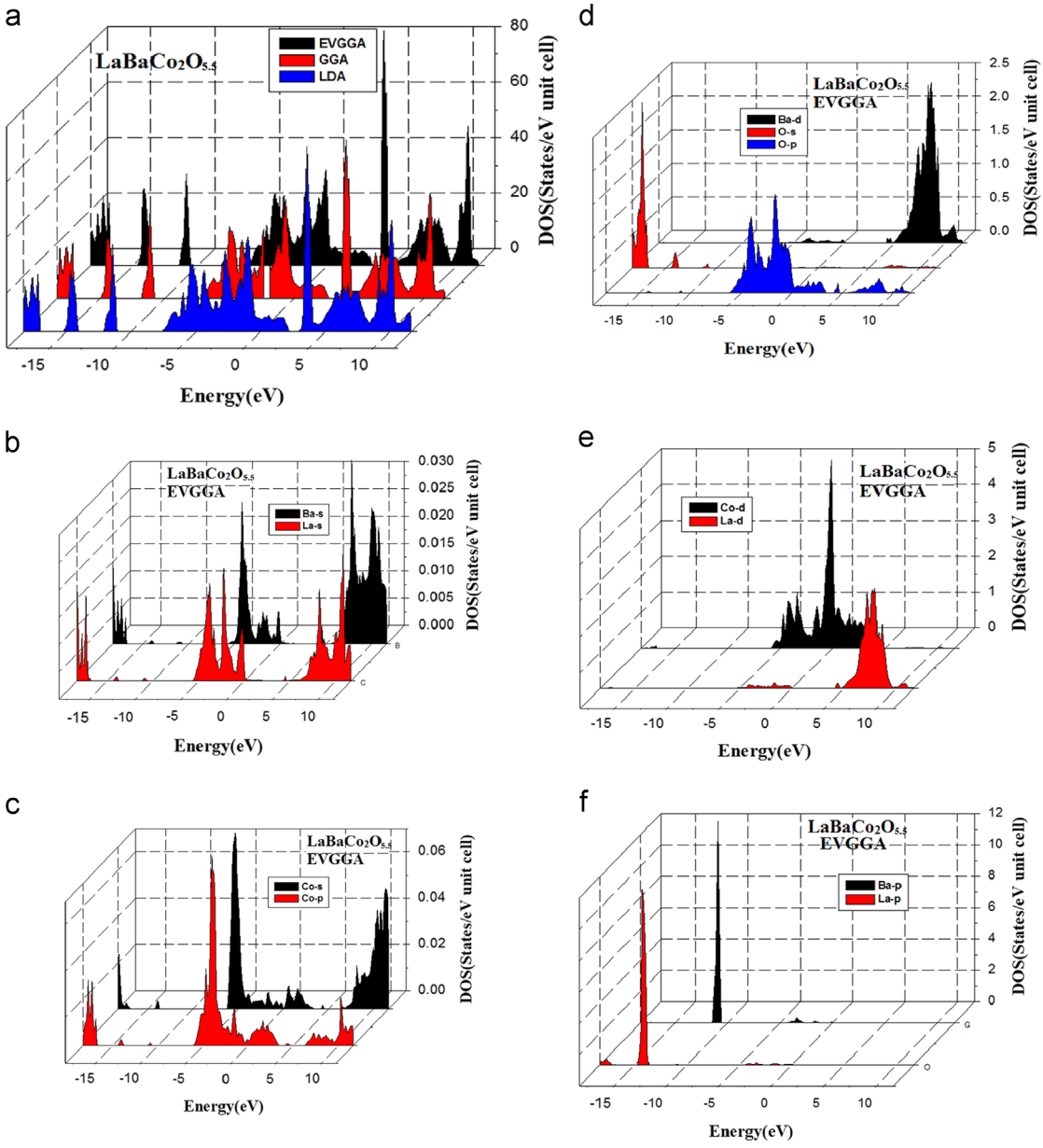

Fig. 3. Partial density of states (PDOS). (a)–(e) Partial density of states only for EVGGA.

considered as key quantities to understand the electronic structure of any metallic material [39–43]. For a better description of the states crossing the Fermi level, we have shown the Fermi surface (FS) of $LaBaCo_2O_{5.5}$ compound. There are five bands (band numbers 110, 111, 112, 113 and 114) across the E_F level. The respective Fermi surface (FS) structures resulting from these five bands are depicted in Fig. 5a–e along with the merged band shown in Fig. 5f. The near-Fermi bands demonstrate a complicated "mixed" character simultaneously with quasi-flat bands along Γ–Z, a series of high dispersive bands intersects the Fermi level. These features yield a multi-sheet FS, which consists (Fig. 5) of two quasi-two-dimensional (2D) electron-like sheets in the corners of the Brillouin zone, and closed disconnected electron-like pockets (around Z) – instead of cylinder-like hole-like sheets for 47 *pmmm* material. Fermi surface defines various electrons in the system, whose topologies are closely related to the transport features of materials, such as electrical conductivity [44,45]. The colors (red, yellow, cerulean and blue) of Fermi surface show variations in electron velocities which are proportional to the superconductivity of the material [46].

In order to understand the nature of chemical bonding for the investigated compound, contour of charge densities in (3 2 0) plane is displayed in Fig. 4. It is clear that a covalent interaction occurs among constituting elements due to the fact that states are degenerate with both angular momentum and lattice site, and also due to the difference in electronegativity between the comprising elements. From the figure, it is clear that the O–Co bond strength is much stronger. In addition there is also a weak interaction between La and Co atoms due to which they are disturbed on the charge density contour around each other. Some ionic character has been noticed from the charge density contour, i.e. Ba and La atoms have ionic bond nature. In fact, the bonding character may be described as a mixture of covalent–ionic and, due to the d-resonance in the vicinity of the Fermi level, is partly metallic. We also calculated the electronic charge density in (1 0 1) plane in order to understand the anisotropy between the two planes. The

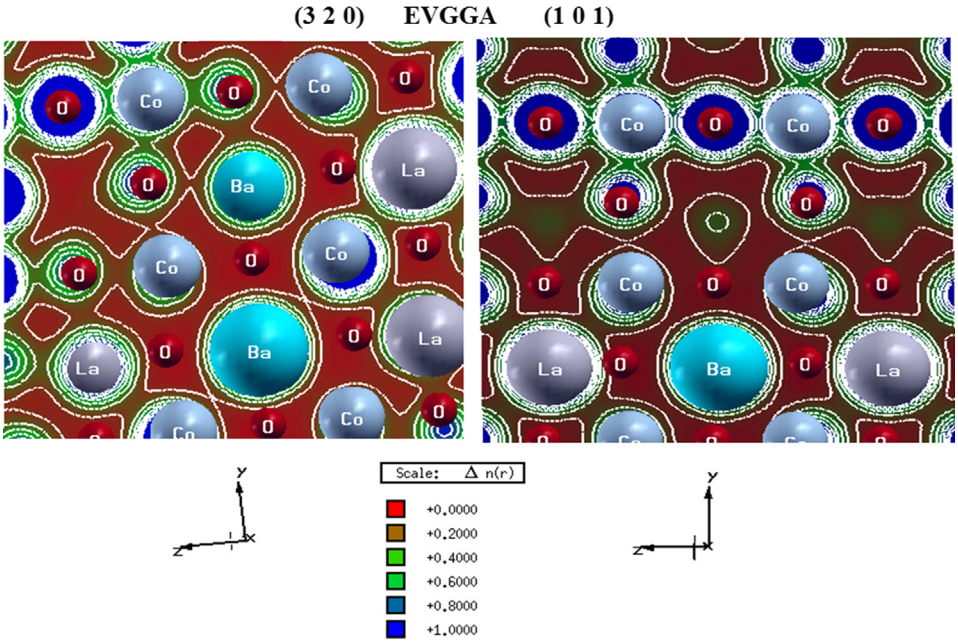

Fig. 4. Electronic charge density (only for EVGGA in (3 2 0) and (1 0 1) plane. (For interpretation of the references to color in this figure legend, the reader is referred to the web version of this article.)

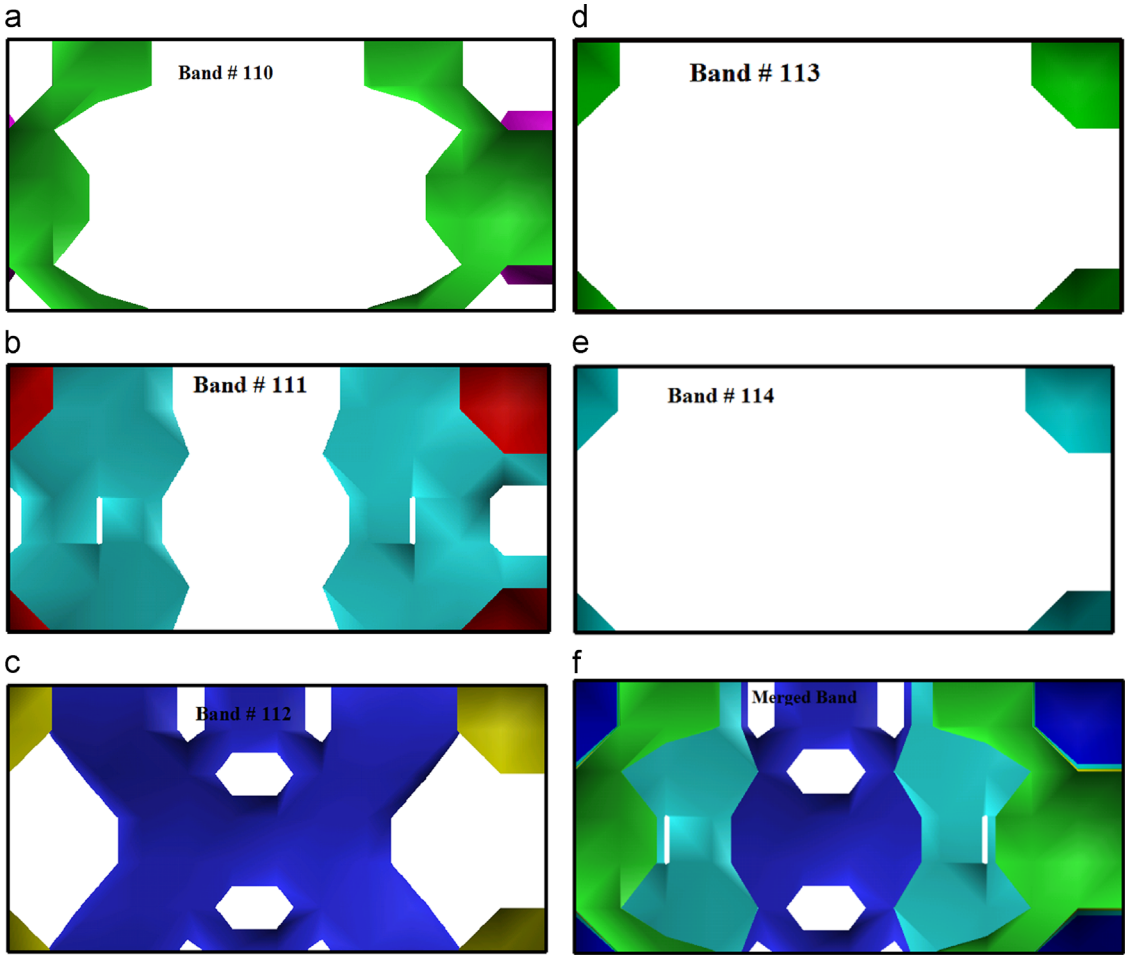

Fig. 5. Fermi surface. (a)–(e) Fermi surface of the five bands. (f) Merged band.

thermo-scale in Fig. 4 shows the intensity of charge density around the atoms, in which blue color shows the maximum charge density while the red color shows the zero charge density. It is clear that the charge density round the Co atom is greater in (3 2 0) than that in (1 0 1) plane. Moreover, O–Co atoms are much closer in (1 0 1) plane than in (3 2 0) plane.

3.2. Optical properties

In Fig. 6, we have displayed the calculated real and imaginary parts of the dielectric function for $LaBaCo_2O_{5.5}$ as a function of the photon energy from 0.0 to 14.0 eV. The dielectric function $\varepsilon = \varepsilon_1 + \varepsilon_2$ spectra will help in accounting for the optical transitions in $LaBaCo_2O_{5.5}$. The imaginary part of the dielectric function, ε_2, was calculated from direct interband transitions using Eq. (1). Fig. 6 shows there is a prominent structure in the imaginary part of the dielectric function of the compound depicted by a peak around 1.0 eV and other smaller humps that decrease in intensity with increase in energy. These structures at about 1.0 eV are associated with direct interband transitions. From band structure results, the transitions originate from the occupied Co d bands below the Fermi level to the unoccupied hybridized Co s/p states above E_F. It is seen that the real part of the dielectric function of the compound has a maximum at less than 1.0 eV and then decreases sharply and passes through zero at about 0.18 eV. This is probably due to strong interband transitions from deeper lying valence bands to unoccupied bands above the Fermi level.

Fig. 7a and b show real and imaginary parts of the optical conductivity $\sigma(\omega) = \sigma_1(\omega) + i\sigma(\omega)$ which is calculated from the dielectric function using Eq. (3). In the spectral region 9.0 to 11.5 eV there exist three maxima in the conductivity spectra which can be assigned to optical transitions from occupied Ba p states to unoccupied La d or Ba d states. The reflectivity spectrum displayed in Fig. 7c is calculated by employing Eq. (4). It is noticed that the reflectivity is over 72% in this compound within the energy range

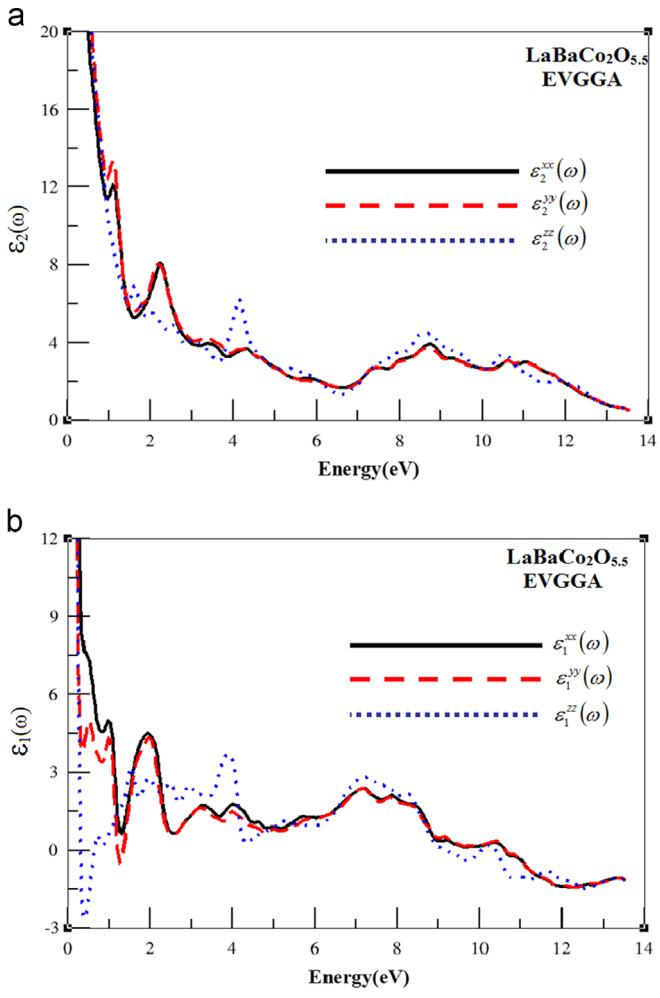

Fig. 6. Optical properties (imaginary (a) and real parts (b).

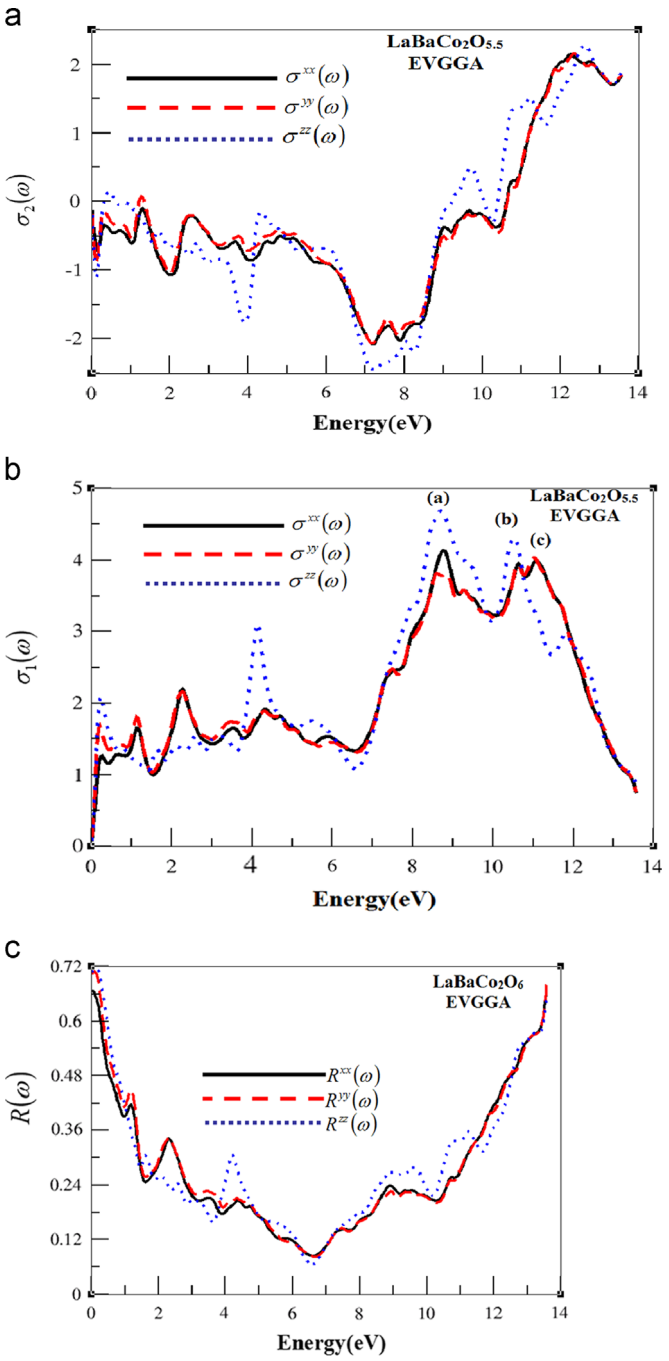

Fig. 7. Evaluation of the related optical properties, namely the reflectivity $R(\omega)$ (b) and conductivity.

studied. This implies that the material will serve as a good reflector. There is however a steady decrease in the reflectivity of the compound with increase in energy to form a valley at 6.8 eV, then again the reflectivity increases.

4. Conclusions

In summary, we have carried out ab-initio calculations of electronic structure, charge density, Fermi surface and optical properties of $LaBaCo_2O_{5.5}$ compound using a full-potential linearized augmented plane-wave method within LDA, GGA and EVGGA schemes. It has been shown that structural parameters obtained after relaxation are in good agreement with the experimental data.

Moreover, the electronic structure showed that $LaBaCo_2O_{5.5}$ compound has a metallic character which allows us to calculate Fermi surfaces. The analysis of charge densities contours reveals that the bonding character in these compounds may result as a mixture between covalent–ionic and metallic behavior. We observe more carefully the calculated optical properties via the calculated optical spectrum, the reflectivity and optical conductivity.

Acknowledgment

The result was developed within the CENTEM project, reg. no. CZ.1.05/2.1.00/03.0088, co-funded by the ERDF as part of the Ministry of Education, Youth and Sports OP RDI programme. Also, Y.A. would like to acknowledge TWAS-Italy for the full support of his visit to JUST-Jordan under TWAS-UNESCO Associateship. Author (R. K.) extends this appreciation to the Deanship of Scientific Research at King Saud University for funding the work through the research group Project no. RGP-VPP-088.

References

[1] C. Martin, A. Maignan, D. Pelloquin, N. Nguyen, B. Raveau, Appl. Phys. Lett. 71 (1997) 1421.
[2] I.O. Troyanchuk, N.V. Kasper, D.D. Khalyavin, H. Szymczak, R. Szymczak, M. Baran, Phys. Rev. Lett. 80 (1998) 3380.
[3] A. Maignan, C. Martin, D. Pelloquin, N. Nguyen, B. Raveau, J. Solid State Chem. 142 (1999) 247.
[4] M. Respaud, C. Frontera, J.L. García-Munõz, M.A.G. Aranda, B. Raquet, J.M. Broto, H. Rakoto, M. Goiran, A. Llobet, J. Rodríguez-Carvajal, Phys. Rev. B 64 (2001) 214401.
[5] Y. Moritomo, T. Akimoto, M. Takeo, A. Machida, E. Nishibori, M. Takata, M. Sakata, K. Ohoyama, A. Nakamura, Phys. Rev. B 61 (2000) R13325.
[6] M. Soda, Y. Yasui, T. Fujita, T. Miyashita, M. Sato, K. Kakurai, J. Phys. Soc. Jpn. 72 (2003) 1729.
[7] J.C. Burley, J.F. Mitchell, S. Short, D. Miller, Y. Tang, J. Solid State Chem. 170 (2003) 339.
[8] A.A. Taskin, A.N. Lavrov, Y. Ando, Phys. Rev. Lett. 90 (2003) 227201.
[9] D.D. Khalyavin, S.N. Barilo, S.V. Shiryaev, G.L. Bychkov, I.O. Troyanchuk, A. Furrer, P. Allenspach, H. Szymczak, R. Szymczak, Phys. Rev. B 67 (2003) 214421.
[10] M. Soda, Y. Yasui, M. Ito, S. Iikubo, M. Sato, K. Kakurai, J. Phys. Soc. Jpn. 73 (2004) 464.
[11] A. Maignan, V. Caignaert, B. Raveau, D. Khomskii, G. Sawatzky, Phys. Rev. Lett. 93 (2004) 26401.
[12] H.D. Zhou, J.B. Goodenough, J. Solid State Chem. 177 (2004) 3339.
[13] A.A. Taskin, A.N. Lavrov, Y. Ando, Phys. Rev. B 71 (2005) 134414.
[14] Z.X. Zhou, P. Schlottmann, Phys. Rev. B 71 (2005) 174401.
[15] M. Baran, V.I. Gatalskaya, R. Szymczak, S.V. Shiryaev, S.N. Barilo, G.L. Bychkov, H. Szymczak, J. Phys.: Condens. Matter 17 (2005) 5613.
[16] Y.P. Chernenkov, V.P. Plakhty, V.I. Fedorov, S.N. Barilo, S.V. Shiryaev, G.L. Bychkov, Phys. Rev. B 71 (2005) 184105.
[17] S. Roy, I.S. Dubenko, M. Khan, E.M. Condon, J. Craig, N. Ali, W. Liu, B.S. Mitchell, Phys. Rev. B 71 (2005) 024419.
[18] V.P. Plakhty, Y.P. Chernenkov, S.N. Barilo, A. Podlesnyak, E. Pomjakushina, E.V. Moskvin, S.V. Gavrilov, Phys. Rev. B 71 (2005) 214407.
[19] W.R. Flawell, A.G. Thomas, D. Tsoutsou, A.K. Mallick, M. North, E.A. Seddon, C. Cacho, A.E.R. Malins, S. Patel, R.L. Stockbauer, R.L. Kurtz, P.T. Sprunger, S.N. Barilo, S.V. Shiryaev, G.L. Bychkov, Phys. Rev. B 70 (2004) 224427.
[20] K. Conder, E. Pomjakushina, V. Pomjakustin, M. Stingaciu, S. Streule, A. Podlesnyak, J. Phys.: Condens. Matter 17 (2005) 5813.
[21] H. Wu, Phys. Rev. B 64 (2000) 092413.
[22] H. Wu, J. Phys.: Condens Matter 15 (2003) 503.
[23] M. Hidaka, M. Soejima, R.P. Wijesundera, M. Soda, M. Sato, S.H. Choi, N.E. Sung, M.G. Kim, J.M. Lee, Phys. Status Solidi B 243 (2006) 1813.
[24] F. Fauth, E. Suard, V. Caignaert, I. Mirebeau, Phys. Rev. B 66 (2002) 184421.
[25] C. Frontera, J.L. García-Munõs, A.E. Carrillo, M.A.G. Aranda, I. Margiolaki, A. Caneiro, Phys. Rev. B 74 (2006) 054406.
[26] D.D. Khalyavin, D.N. Argyriou, U. Amann, A.A. Yaremcmhenko, V.V. Kharton, Phys. Rev. B 75 (2007) 134407.
[27] S.N. Barilo, S.V. Shiryaev, G.L. Bychkov, A.S. Shestak, W.R. Flavell, A.G. Thomas, H.M. Rafique, Y.P. Chernenkov, V.P. Plakhty, E. Pomjakushina, K. Conder, P. Allenspach, J. Cryst. Growth 310 (2008) 1867.
[28] C. Frontera, J.L. García-Munõs, O. Castanõ, C. Ritter, A. Caneiro, J. Phys.: Condens. Matter 20 (2008) 104228.
[29] J.E. Jorgensen, L. Keller, Phys. Rev. B 77 (2008) 024427.
[30] D.D. Khalyavin, D.N. Argyriou, U. Amann, A.A. Yaremchenko, V.V. Kharton, Phys. Rev. B 77 (2008) 064419.
[31] E.L. Rautama, V. Caignaert, P.h. Boullay, K. Asias Kundu, V. Pralong, M. Karppinen, C. Ritter, P. Raveau, Chem. Mater. 21 (2009) 102–109.
[32] T. Satyanarayana, I.V. Kityk, M. Piasecki, P. Bragiel, M.G. Brik, Y. Gandhi, N. Veeraiah, J. Phys.: Condens. Matter 21 (24) (2009) 245104.
[33] P. Blaha, K. Schwarz, J. Luitz, WIEN97: A Full Potential Linearized Augmented Plane Wave Package for Calculating Crystal Properties, Techn. Universit at Wien, Austria, ISBN 3-9501031-0-4, 1999.
[34] J.P. Perdew, A. Zunger, Phys. Rev. B 23 (1981) 5048.
[35] J.P. Perdew, K. Burke, M. Ernzerhof, Phys. Rev. Lett. 77 (1996) 3865.
[36] E. Engel, S.H. Vosko, Phys. Rev. B 50 (1994) 10498.
[37] A. Delin, P. Ravindran, O. Eriksson, J.M. Wills, Int. J. Quantum Chem. 69 (1998) 349.
[38] W.T. Ching, P. Rulis, Phys. Rev. B 73 (2006) 045202.
[39] S. Azam, A.H. Reshak, Physica B 431 (2013) 102–108.
[40] A.H. Reshak, S. Azam, J. Magn. Magn. Mater. 352 (2014) 72–80.
[41] A.H. Reshak, S. Azam, J. Magn. Magn. Mater. 345 (2013) 294–303.
[42] A.H. Reshak, S. Azam, J. Magn. Magn. Mater. 342 (2013) 80–86.
[43] A.H. Reshak, S. Azam, J. Magn. Magn. Mater. 351 (2014) 98–103.
[44] A.H. Reshak, S. Azam, J. Magn. Magn. Mater. 358–359 (2014) 16–22.
[45] A.H. Reshak, S. Azam., Int. J. Electrochem. Sci. 8 (2013) 10396–10423.
[46] A.H. Reshak, S.A. Khan, J. Magn. Magn. Mater. 354 (2014) 216–221.